UNITED NATIONS UNIVERSITY
GEOTHERMAL TRAINING PROGRAMME
Orkustofnun, Grensasvegur 9,
IS-108 Reykjavik, Iceland

Reports 2013
Number 26

RESISTIVITY STRUCTURE OF THE EBURRU GEOTHERMAL FIELD, KENYA, DEPICTED THROUGH 1D JOINT INVERSION OF MT AND TEM DATA

Ammon Ojwang Omiti
Kenya Electricity Generating Company Ltd. - KenGen
Geothermal Resource Development
P.O. Box 785
Naivasha 20117
KENYA
aomiti@kengen.co.ke

ABSTRACT

Eburru is one of the geothermal fields in Kenya, producing 2.5 MWe from one of the six exploratory wells. In order to drill production wells, a total of 36 additional MT and TEM soundings were carried out in 2013 to delineate the geothermal resource field of Eburru. This report discusses and presents the results of earlier soundings and soundings from 2013 which brought the total number to 43 MT and 43 TEM soundings. The TEMTD program was used for joint 1D inversion of MT and TEM data, the program calculates the shift factor. The MT data are, therefore, corrected for static shift. Data used in this report were acquired by the KenGen staff team using a data logger MTU-5A made by Phoenix Ltd. for acquiring MT data and TerraTEM made by Monex GeoScope Ltd. for TEM data. MT data were processed using SSMT2000 and MTEditor before jointly inverted with TEM data. The results discussed in this report present 1D joint inversion, resistivity cross-sections and iso-resistivity maps down to a few kilometres. The reservoir in Eburru geothermal field is located at about 2500 m b.g.l. according to the sub-surface resistivity structure.

1. INTRODUCTION

Eburru geothermal field is located in the great East African Rift System (EARS) which is a major tectonic structure stretching about 6100 km starting from the Red Sea in the north to Mozambique in the south. The Rift starts from a triple junction, evident in Ethiopia; at this point, two branches are in contact with the Red Sea and the Gulf of Eden while the third passes through Ethiopia to the south. Eburru is located in the eastern arm of the EARS stretching though Eritrea, Ethiopia, Kenya, and all the way down to Mozambique (Figure 1). The Great Africa Rift system forms more or less a linear like zone where the continental plate is being pulled apart with the rifting between. A widened mantle plume probably began under east Africa creating the three arms which are: The East Africa Rift, The Gulf of Eden Rift and The Red Sea Rift (Omenda and Karingithi, 1993). The heat flow from the asthenosphere along the rift zones led to volcanism and the formation of domes, as can be seen in Olkaria to the south of Eburru (Figure 2). The eastern branch is believed to be much older and is considered to have developed about 13-23 million years earlier than the western branch; this is supported by the discovery of preserved vertebrate fossils and volcanic ash which are believed to be about 23 million years old (Velador et al., 2002).

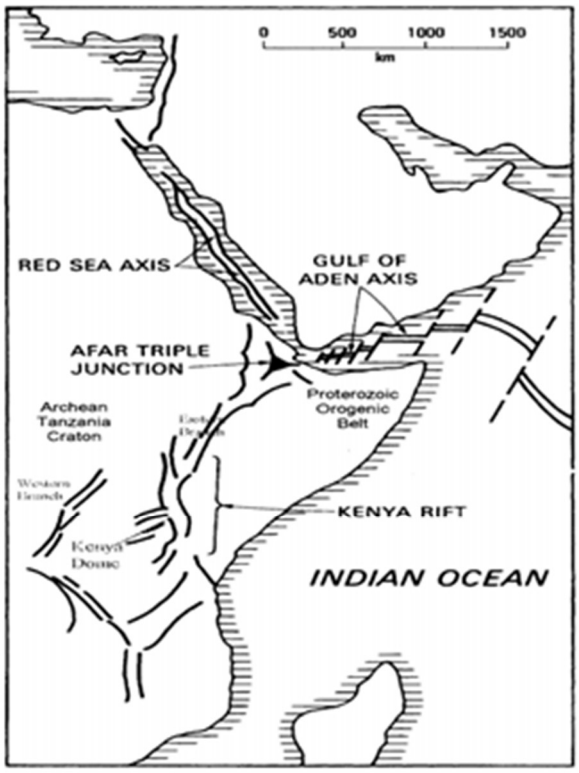

FIGURE 1: Location map of the East African Rift (Clarke et al., 1990)

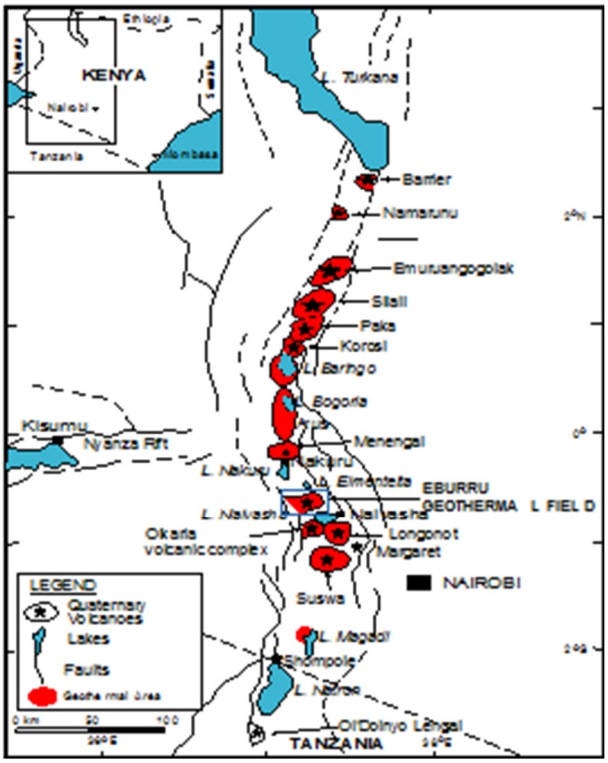

FIGURE 2: Map showing the location of Eburru geothermal field (name shown in blue box) in the Kenya Rift system

The stretching caused fracturing above the ductile brittle boundary leading to the formation of a series of normal faults and, hence, the graben structure along the Rift valley. The continuous stretching process is associated with thinning of the crust and volcanic eruptions, often forming caldera as seen in Eburru and lava flows covering large areas with some exposed on the Rift valley flanks. The EARS largely follows the ancient continental plates that collided to form the African craton billions of years ago.

2. RESISTIVITY OF ROCKS

2.1 Specific resistivity

The specific resistivity of a material, ρ (Ωm), is given in terms of the resistance R (Ω) for current flow along a bar of length l and cross-sectional area A by the formula:

$$\rho = \frac{RA}{l} \tag{1}$$

where ρ = Specific resistivity (Ωm);
R = Resistance (Ω);
A = Area (m^2);
l = Length (m).

Conductivity (σ) is the reciprocal of resistivity measured in Siemens/m (S/m) and vice versa. Resistivity of soil or rock is affected by temperature, salinity of the pore water, water rock interaction, porosity and permeability.

2.2 Porosity

Fractional porosity, ϕ_τ, is defined as the fraction of void space of a given total volume of a rock material or the measure of the ability of a given rock material to hold fluid:

$$\phi_\tau = \frac{V_\theta}{V} \tag{2}$$

where ϕ_τ = Fractional porosity;
V_θ = Volume of void;
V = Total volume of the material.

Archie's law has been used for relating the conductivity of a reservoir rock and the conductivity of the fluid contained in the pores. It describes the resistivity dependence on porosity if ionic conduction in the pore fluid dominates other conduction mechanisms in the rocks. For normal rocks, the law is valid only if the resistivity of pore fluid is 2 Ωm or less and it is a very good approximation if the resistivity is dominated by the saturating fluid (Archie, 1942):

$$\rho = \rho_w a \phi_\tau^{-n} \tag{3}$$

where ρ_w = Resistivity of the pore fluid (Ωm);
ϕ_τ = Fractional porosity;
a = Empirical parameter;
n = Cementing factor.

2.3 Temperature

Resistivity of an electrolyte and temperature are related as shown in Figure 3. The resistivity of rock decreases with increasing temperature, more ions are set free and a decrease in the viscosity of the electrolytic solution makes them more mobile. At higher temperatures, above 300°C, a decrease in dielectric permittivity of water results in a decrease in the number of dissociated ions in the solution, hence, an increase in fluid resistivity.

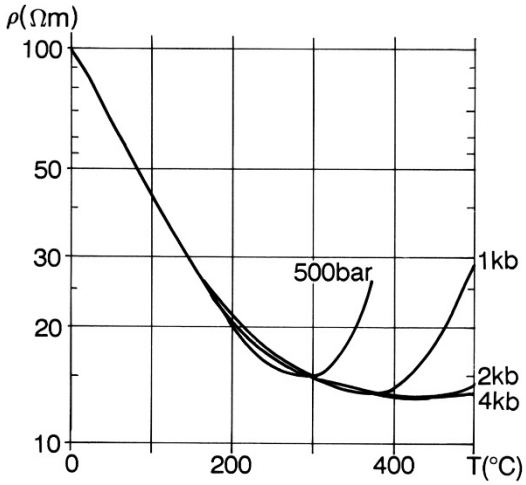

FIGURE 3: Electrical resistivity of NaCl solution as a function of temperature at different pressures (Hersir and Björnsson, 1991; based on Quist and Marshall, 1968)

Dakhnov (1962) described the relationship between temperature and resistivity of an electrolyte for temperatures in the range of 0 to about 200°C with the formula:

$$\rho_w = \frac{\rho_{wo}}{1 + \alpha(T - T_0)} \tag{4}$$

where ρ_w = Resistivity (Ωm) of the fluid at temperature T;
ρ_{wo} = Resistivity (Ωm) of the fluid at temperature T_0;
T_0 = Room temperature (°C);
α = Coefficient temperature of the resistivity, $\alpha \approx 0.023°C^{-1}$ for T_0= 25°C.

The importance of temperature variation of electrolytes on the resistivity of rocks is greatest at temperatures below 150°C but decreases with an increase in temperatures due to mineral alteration.

2.4 Salinity of pore fluid

Dissolved salts in water normally break into negatively and positively charged ions. In saline water, positively charged ions are calcium (Ca^{+}), sodium (Na^{+}), Magnesium (Mg^{+}) and potassium (K) while the negatively charged ions are sulphate (SO_4^{-2}), carbonate (CO_3^{-2}), chloride (Cl^{-}) and bicarbonate (HCO_3^{-}). Salinity is the practical measure of the amount of dissolved salts in water. The relationship between conductivity and salinity is described by the equation below (Zhdanov and Keller, 1994):

$$\sigma = \frac{1}{\rho} = \mathrm{F} \cdot (c_1 q_1 m_1 + c_2 q_2 m_2 + \ldots) \quad (5)$$

where σ = Conductivity (S/m);
F = Faraday's number (9.65 x 10^4 C/mole);
c_i = Concentration of ions;
q_i = Valence of ions;
m_i = Mobility of ions.

Conductivity of the rock increases with increased salinity of the pore fluid.

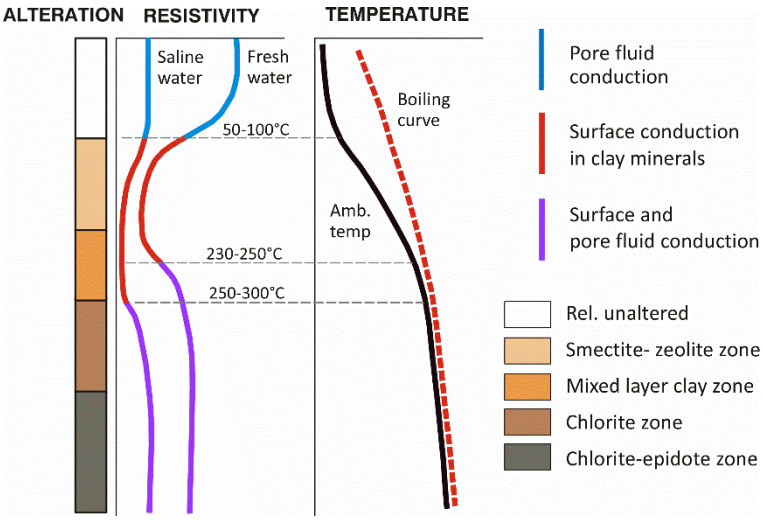

FIGURE 4: A summary of general resistivity structure of high temperature fields in Iceland (Flóvenz et al., 2012; based on Flóvenz et al., 2005)

2.5 Water rock interaction

The interaction between hot fluids and rocks results in the formation of secondary minerals which is called geothermal alteration. The main factors determining which type of alteration is formed are fluid composition, permeability and temperature (Henley and Ellis, 1983). The secondary minerals at medium to low temperature in basalt are commonly dominated by clays (smectite and illite), zeolites, oxides (Meheganet al., 1982), and hydroxides. At temperatures of about 200-250°C a zone of mixed clays is formed, then replaced by chlorite and epidote at 250-300°C. At temperatures greater than 300°C (Figure 4) epidote and actinolite become common.

The resistivity of the reservoir rock is dependent on the minerals present. The resistivity of the chlorite-epidote zone increases due to low mobility of ions bound in a crystal lattice.

3. ELECTRICAL RESISTIVITY METHOD

Electrical resistivity methods are used to measure the resistivity structure of the subsurface. Current is induced into the ground and signals are monitored at the surface. The following are the most common resistivity methods:

- DC resistivity methods
- Electromagnetic methods

3.1 Direct current resistivity method

The direct current (DC) resistivity method is one of the techniques used to measure the earth's resistivity; by making a measurement on the ground surface, the true resistivity of the ground can be estimated. Current is driven into the ground and the resulting voltage is measured at the surface.

Figure 5 describes the basic principles of DC resistivity measurements. Current is injected through a pair of electrodes (A and B) which are short metallic stakes driven about two feet into the ground; two additional electrodes (M and N) are then used to measure the resulting potential difference (V) generated by the current (I).

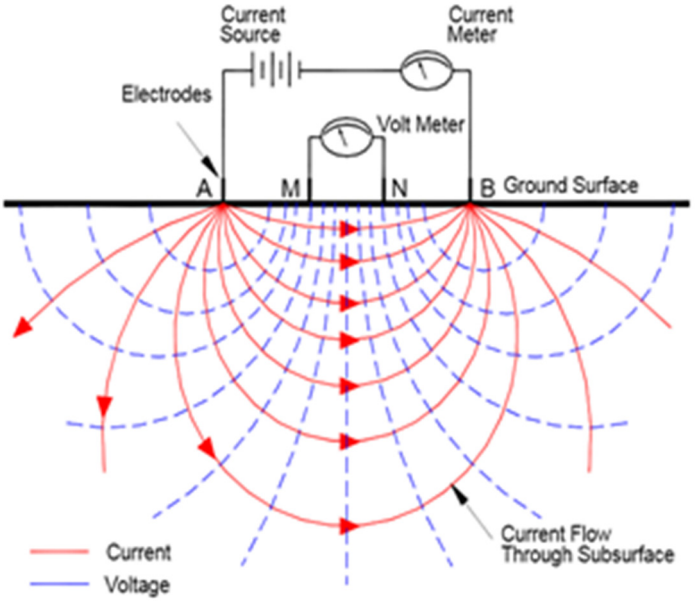

FIGURE 5: Illustrating schematic basic concept of direct current resistivity measurement

Readings obtained from the instrument (current and voltage) are normally reduced to apparent resistivity values. Apparent resistivity is defined as the resistivity of the earth that would produce the observed instrument result or response for a given distance of electrode spacing and is normally plotted on a log-log graph.

Ohm's law is a fundamental physical law governing the flow of current in the ground:

$$\boldsymbol{J} = \sigma \boldsymbol{E} = \frac{1}{\rho}\boldsymbol{E} \tag{6}$$

where $\boldsymbol{J}$ = Current density (A/m^2);
$\boldsymbol{E}$ = Electric field intensity (V/m);
σ = Conductivity of the medium (Ωm)$^{-1}$;
ρ = Resistivity (Ωm).

The potential from a point source is given by:

$$V(r) = \frac{\rho I}{2\pi r} \tag{7}$$

where V = Potential (V);
r = Distance to the current electrode (m);
I = Total current flow (A).

Potentials measured at M and N in Figure 5 in a linear array are given by:

$$V_M = \frac{\rho I}{2\pi}\left(\frac{1}{AM} - \frac{1}{MB}\right) \tag{8}$$

$$V_N = \frac{\rho I}{2\pi}\left(\frac{1}{AN} - \frac{1}{NB}\right) \tag{9}$$

Total potential difference between electrode M and N is, thus:

$$V_{MN} = V_M - V_N = \frac{\rho I}{2\pi}\left[\left(\frac{1}{AM} - \frac{1}{MB}\right) - \left(\frac{1}{AN} - \frac{1}{NB}\right)\right] \tag{10}$$

The above equation can be rearranged to yield:

$$\frac{2\pi}{K} = \left[\left(\frac{1}{AM} - \frac{1}{MB}\right) - \left(\frac{1}{AN} - \frac{1}{NB}\right)\right] \tag{11}$$

The resistivity is, therefore, equal to:

$$\rho = \frac{V_{MN}}{I} K = \frac{V_{MN}}{I} \pi \left[\frac{S^2 - P^2}{2P}\right] \tag{12}$$

where S = Half distance between A and B (m);
P = Half distance between M and N (m).

For a non-homogeneous earth, Equation 12 is used to define the apparent resistivity which is a function of S and P. For the Wenner array there is equidistance separation between the electrodes a; the geometric factor of the Wenner array assumes a simple form, $K = 2\pi a$, hence the apparent resistivity is equal to:

$$\rho_{Wenner} = \left(\frac{V_{MN}}{I}\right) 2\pi a \tag{13}$$

3.2 Electromagnetic methods

In electromagnetic measurements, an alternating magnetic field is used to induce measurable current in the subsurface. The method includes time domain electromagnetic and frequency domain electromagnetic methods. Primary fields are generated by passing alternating current (AC) through long wires or loops, inducing eddy currents which generate secondary fields depending on the resistivity of the subsurface rocks.

3.2.1 Transient electromagnetic method (TEM)

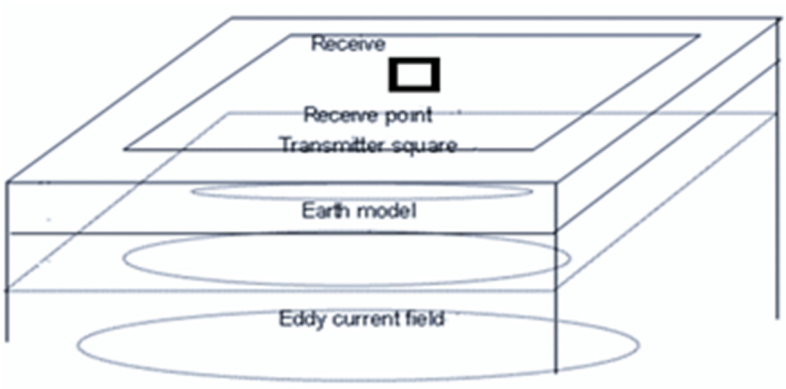

FIGURE 6: Central loop TEM sounding configuration

The transient electromagnetic method (TEM) is used to measure the electrical resistivity of the subsurface down to a depth of several hundreds of metres. The measurements can be conducted on the ground (Figure 6) or can be air-born (skyTEM) to cover a large area over a short period of time. The TEM is executed by passing current into the ungrounded TX-loop to build up a known constant magnetic field, termed the primary magnetic field. The current is abruptly turned off and the change in the primary magnetic field induces electromotive force which results in eddy currents in the surroundings which, again, result in a secondary magnetic field.

The secondary magnetic field from the eddy currents decreases with time as the eddy currents diffuse downwards and outwards. The resistance of the country rocks weakens the current with time, converting the electrical energy to heat. The decay rate of the magnetic field is measured as the voltage induced into the receiver coil at the centre of the transmitter loop.

Maxwell's equations are used to define the fundamental law of the electromagnetic field (Kaufman and Keller, 1983):

$$\boldsymbol{\nabla} \times \boldsymbol{E} = -\frac{\partial \mathbf{B}}{\partial t} \tag{14}$$

$$\boldsymbol{\nabla} \times \boldsymbol{H} = \boldsymbol{j} + \frac{\partial \boldsymbol{D}}{\partial t} \tag{15}$$

$$\boldsymbol{\nabla} \cdot \mathbf{B} = 0 \tag{16}$$

$$\boldsymbol{\nabla} \cdot \boldsymbol{D} = \eta \tag{17}$$

For isotropic medium the described fields above are linked with:

$$\boldsymbol{D} = \varepsilon \boldsymbol{E} \tag{18}$$

$$\boldsymbol{B} = \mu \boldsymbol{H} \tag{19}$$

$$\boldsymbol{j} = \sigma \boldsymbol{E} \tag{20}$$

where $\boldsymbol{E}$ = Electrical intensity (V/m);
η = Electric charge density of free charges (C/m^3);
$\boldsymbol{D}$ = Electric displacement vector (C/m^2);
$\boldsymbol{B}$ = Magnetic flux density (*T);*
$\boldsymbol{j}$ = Electric current density (A/m^2);
$\boldsymbol{H}$ = Magnetic field (A/m);
μ = Magnetic permeability (H/m);
ε = Electric permittivity (F/m);
σ = Electrical conductivity (S/m).

In a homogeneous half space of conductivity (σ), the induced voltage in the receiver coil at late times is (Árnason, 1989):

$$V(t,r) \approx I_o \frac{C(\mu_o \sigma \, \mathrm{r}^2)^{\frac{3}{2}}}{10\pi^{\frac{1}{2}} t^{\frac{5}{2}}} \tag{21}$$

where C = $A_r n_r A_s n_s \frac{\mu_o}{2\pi^3}$;
t = Time elapsed after the transmitter current is turned off (s);
A_r = Cross-sectional area of the receiver loop (m^2);
A_s = Cross-sectional area of the transmitter loop (m^2);
n_s = Number of windings in the transmitter loop;
r = Radius of the transmitter loop;
$V(t,r)$ = Transient voltage (V);
I_o = Current in the transient loop (A).

The late time apparent resistivity (ρ_a) is defined by solving Equation 21, leading to Equation 22:

$$\rho_a = \frac{\mu_o}{4\pi}\left[\frac{2I_o\mu_o A_r A_s n_r n_s}{5t^{\frac{5}{2}}\mathrm{V}(t,r)}\right]^{2/3} \tag{22}$$

3.2.2 Magnetotelluric method (MT)

The magnetotelluric method (MT) is a passive electromagnetic method that measures the electrical properties below the earth's surface. Natural variation in the earth's magnetic field is the source of energy for the magnetotelluric technique. The primary magnetic field, which is the external energy, is generated by variations in the earth's magnetic field transferred in a wide and continuous spectrum of electromagnetic waves. On reaching the earth's surface, some are reflected and the remaining part penetrates into the earth and induces currents (telluric current) into the earth. The telluric currents produce a secondary magnetic field which is measured on the earth's surface providing information on the conductivity of the subsurface up to hundreds of kilometres in depth.

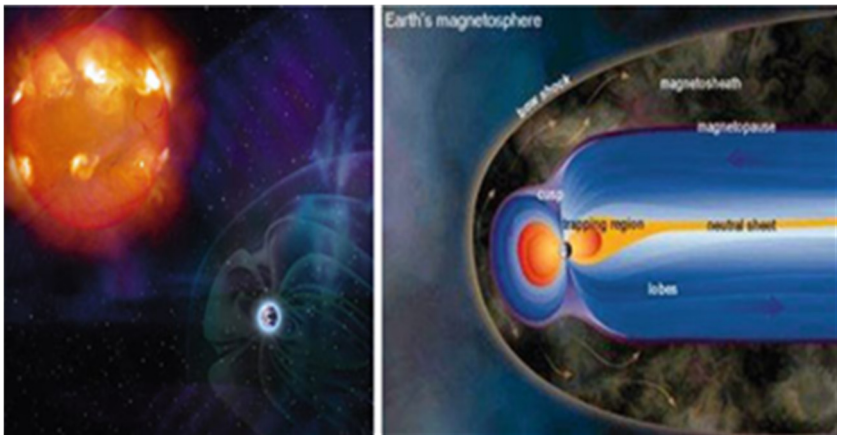

FIGURE 7: Solar wind interaction with the magnetosphere (Encyclopaedia Britannica, 2010)

Frequencies above 1 Hz are generated by lightening discharge along equatorial regions and frequencies lower than 1 Hz are generated by the interaction of the earth's magnetosphere and solar winds (Figure 7). Solar wind is a continual stream of plasma radiating mainly protons and electrons from the sun and when it encounters magnetopause, they are deflected in opposite directions, establishing an electric field.

Maxwell's equations describe the electromagnetic field within a material (Equations 14-17), and have solutions as a linear combination of harmonic waves:

$$E = E_o e^{i(\omega t + kr)} \tag{23}$$

$$B = B_o e^{i(\omega t + kr)} \tag{24}$$

where ω = Angular frequency of electromagnetic oscillations (rad/s);
t = Time (s);
k = Wave number (m^{-1});
r = Position vector (m).

In a homogeneous structure the electric component takes the form:

$$E = E_o e^{i\omega t} \cdot e^{-i\beta z} \cdot e^{-\alpha z} \tag{25}$$

where β = $\sqrt{\mu\sigma\omega/2}$ (m^{-1}).

The first factor of Equation 25 is wave amplitude, the second and third factors are sinusoidal time and variation in depth, respectively, and the last one is exponential decay.

Skin depth can be defined as the depth where the electromagnetic field has been reduced to e^{-1} of the original value. The decay can be expressed by skin depth, δ (m), and for the value of z which in this case decays to 1/e (Vozoff, 1991):

$$\delta = \sqrt{(2/\mu_o)\sigma\omega} = 500\sqrt{\rho T}\ (m) \tag{26}$$

The skin depth permits the characterization of the investigated depth to increase according to the square root of the product of period and resistivity.

Uniform half space
If a uniform half space is impinged upon by a vertically propagating (along z-axis) plane electromagnetic wave $\partial E/\partial x = \partial H/\partial x = \partial E/\partial y = \partial H/\partial y = 0$, and the fields obey equations like:

$$\frac{\partial^2 E_x}{\partial z^2} = k^2 E_x \tag{27}$$

where $k^2 = i\mu\sigma\omega$.

From Maxwell´s equations we get:

$$H_y = -\frac{1}{i\mu\omega}\frac{\partial E_x}{\partial z} \tag{28}$$

The orthogonal components of the field satisfy:

$$Z = \frac{E_x}{H_y} = \frac{i\omega\mu}{k} = -\frac{E_y}{H_x} \tag{29}$$

The relationship between the electric and magnetic fields is, therefore:

$$\begin{pmatrix} E_x \\ E_y \end{pmatrix} = \begin{pmatrix} 0 & Z \\ -Z & 0 \end{pmatrix} \begin{pmatrix} H_x \\ H_y \end{pmatrix} \tag{30}$$

where

$$Z = \sqrt{(i\omega\mu)/\sigma} \tag{31}$$

A magnetic field lags behind the electric field by $\pi/4$ in a completely homogeneous and isotropic half space with true resistivity equal to:

$$\rho = \frac{|Z|^2}{\omega\mu} = \frac{T}{2\pi\mu}|Z|^2 \tag{32}$$

where T = The period (s).

This can be expressed as (Cagniard, 1953):

$$\rho = 0.2\,T\frac{|E_x|^2}{|H_y|^2} \tag{33}$$

where ρ = Resistivity (Ωm);
T = Period (s);
E = Horizontal electric field (mV/km);
H = Orthogonal horizontal magnetic field in γ = Tesla $\cdot 10^{-9}$.

For inhomogeneous half space, the above equation is used to define the apparent resistivity:

$$\rho_a = 0.2\,T|Z|^2 = \frac{|E|^2}{|H|^2} \tag{34}$$

Z also has a phase:

$$\varphi = tan^{-1}\frac{(\text{image}\left[\frac{E_x}{H_y}\right])}{(\text{Real}\left[\frac{E_x}{H_y}\right])} \tag{34}$$

Tensor impedance
1D impedance tensor: The conductivity of a 1D layered earth changes only with depth. The impedance tensor, Z, in this case is expressed as:

$$Z_{1D} = \begin{pmatrix} 0 & Z_{xy} \\ -Z_{xy} & 0 \end{pmatrix} \tag{35}$$

The apparent resistivity and phase in a layered earth are defined as:

$$\rho_a(\omega) = \frac{1}{\omega\mu_o}|Z(\omega)|^2 \; and \; \varphi = \tan^{-1}\left[\frac{ImZ_{xy}}{ReZ_{xy}}\right] \tag{36}$$

2D impedance tensor: The conductivity for a 2D earth changes in one lateral direction and with depth but is constant in strike the direction:

$$\mathrm{Z}_{2D} = \begin{pmatrix} Z_{xx} & Z_{xy} \\ Z_{yx} & Z_{yy} \end{pmatrix} \tag{37}$$

The horizontal axes of the field layout are normally not aligned along the electromagnetic strike. The diagonal elements $Z_{xx} = -Z_{yy}$ are equal in amplitude but have opposite signs; the off diagonal Z_{xy} and Z_{yx} are independent values. If the x direction is parallel to the strike direction, Z_{2D} impedance tensor becomes:

$$\mathrm{Z}_{2D} = \begin{pmatrix} 0 & Z_{xy} \\ Z_{yx} & 0 \end{pmatrix} \tag{38}$$

The strike direction in a 2D earth is obtained by rotating the coordinates system to the direction minimizing the diagonal elements of the tensor, Z_{xx} and Z_{yy}. The 90° ambiguity in the electric strike is resolved by calculating the Tipper strike from H_z.

3D impedance tensor: The conductivity in a 3D earth varies in all directions (*x, y and z).* The impedance tensor in this case is expressed as:

$$\mathrm{Z}_{3D} = \begin{pmatrix} Z_{xx} & Z_{xy} \\ Z_{yx} & Z_{yy} \end{pmatrix} \tag{39}$$

All the elements of the 3D impedance tensor must all be considered, because they are non-zero irrespective of rotation.

According to Flóvenz et al. (2012), it is very essential in a 1D dimension to invert for some rotational invariants defined in such a way that it averages over directions. Then one does have to deal with the question of rotation. Three such invariants exist:

$$Z_B = \frac{Z_{xy} - Z_{yx}}{2} \tag{40}$$

$$Z_{det} = \sqrt{Z_{xx}Z_{yy} - Z_{xy}Z_{yx}} \tag{41}$$

$$Z_{gm} = \sqrt{-Z_{xy}Z_{yx}} \tag{42}$$

All these parameters give the same values for a 1D earth response. For 2D, Z_{det} (determinant) and Z_{gm} (geometric mean) reduce to the same value, but Z_B (arithmetic mean) is different. For 3D responses, all these parameters are different (Flóvenz et al., 2012).

Tipper

For a non-1D earth, a part of the magnetic field tips into the vertical. The vertical magnetic component H_z is expressed as a linear combination of horizontal magnetic field components H_x and H_y (Everett and Hyndman, 1967), where:

$$H_z = AH_x + BH_y \tag{43}$$

The Tipper magnitude is given by:

$$T = \sqrt{A^2 + B^2} \tag{44}$$

For a 1D earth, $A = B = 0$. For a 2D earth the structure can be rotated such that the x-axis is in the strike direction where $A = 0$, but $B \neq 0$. This is done by properly minimizing$|A|$. This strike direction is called the Tipper strike.

Shift
Static shift is frequency independent off-set or shift of the apparent resistivity curves when plotted on a log-scale (constant multiplicative factor on a linear scale) scaled by a real factor. It results from distortion of the amplitude of the electric field due to the presence of shallow and local bodies of non-homogeneities. The scaling factor of shift cannot be determined from MT data collected at one station. A reliable indicator that static shift is present in the data is a parallel shift of apparent resistivity curves for ρ_{xy} and ρ_{yx}. Lack of parallel shift of apparent resistivity does not guarantee absence of static shift since the scaling factor of the two curves might be equal.

Interpretation of MT data via 1D modelling without considering the static shift will shift the depths of conducting bodies by the square root of the shift factors, and modelled resistivity will be wrong by a factor of S.

4. INSTRUMENTATION OF MAGNETOTELLURIC AND TRANSIENT ELECTRO-MAGNETIC EQUIPMENT

4.1 Magnetotelluric (MT) equipment

Magnetotelluric (MT) equipment is used for data acquisition and the main aim is to collect high quality data over a broad period range. The equipment consists of three magnetic sensors, five electrodes, five telluric cables each at least 30 m long, magnetic cables and one data logger; usually a five channel logger is used to measure the time components of the electromagnetic field, E_x, E_y, H_x, H_y and H_z. The deployment of MT equipment is done in reference to the x and y-axis in magnetic north and east, respectively. The E-fields are measured as voltage between rounded electrodes about 60 m (2 × 30 m) apart. The electrode at the centre is used to ground the data logger (Figure 8). The magnetic coil for H_x is oriented along the magnetic N-S direction with the connected side facing the instrument (Figure 9); H_y is oriented along the magnetic E-W direction and H_z is the vertical component. The electrodes are connected to the MTU data logger. The electrodes are made of KCl or $PbCl_2$ in solution enclosed in a ceramic container. Wet bentonite is applied on the outside of the electrodes to ensure good contact with the soil. The three magnetic coils measure the natural time varying magnetic fields at the earth´s surface which are caused by electromagnetic waves radiated from the sun and from distant electrical storms (Vozoff, 1991). The soundings were made by computing the impedance for a range of frequencies ranging from 320 to 0.001 Hz from data acquired over 18-26 hours.

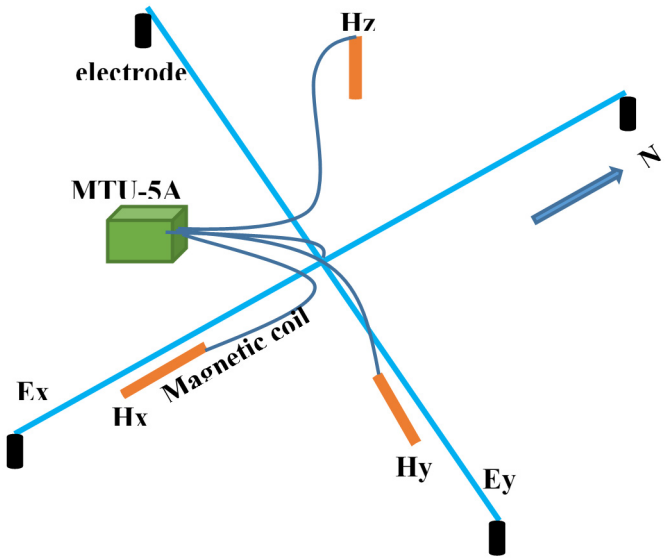

FIGURE 8: Layout of MT equipment (each electrode is placed 30 m from centre of the array)

FIGURE 9: Magnetic N-S trending magnetic coil

4.2 Transient electromagnetic method (TEM)

The instrument used in the acquisition of the analysed data was TerraTEM, developed by MonexGeoScope Pty Ltd. TerraTEM is made up of a transmitter (TX), receiver (RX), a 100×100 m loop and a battery pack. The transmitter is connected to the loop and the receiver placed at the centre is also connected to the transmitter with a synchronization cable (Figure 10).

The data used in this report were acquired according to the method developed by Monex Ltd. The locations of the loops were always chosen depending on area topography, avoidance of cultural interference and accessibility. The loop was laid out using compass directions to measure the sides precisely. All the data collected by TerraTEM were processed using TerraTEM software and stored in USF form before being taken to TEMTD for inversion.

5. GEOTHERMAL SURVEY AT EBURRU GEOTHERMAL FIELD

5.1 Geology of Eburru

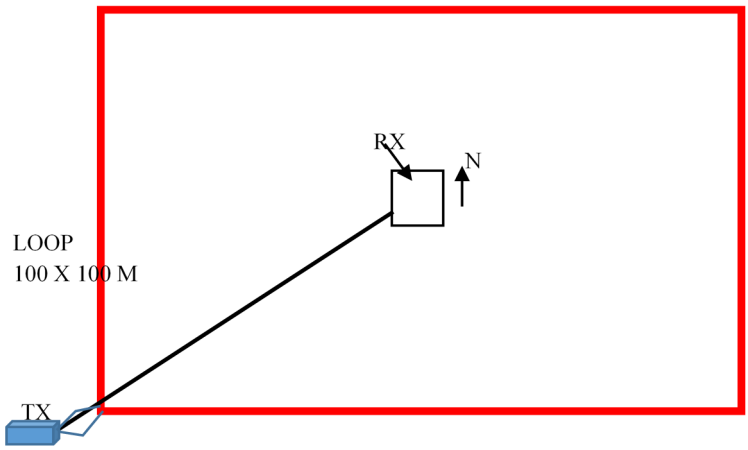

FIGURE 10: Schematic diagram of TerraTEM equipment deployed in the field

Eburru geothermal field is located within the Great Rift Valley system to the south of Menengai and north of Olkaria geothermal fields. In the 1980s, geoscientific studies were done in Eburru leading to the drilling of six exploratory wells between 1986 and 1990 with an average depth of 2.5 km. The elevation reaches 2800 m above sea level and is the highest topography within the Rift valley floor. Eburru structures mainly trend in N-S direction with west and east volcanic centres. Eburru has been active since Pleistocene. Rhyolite, trachytes and basalts are the most abundant rocks in the area and trachytes are mainly pantelleritic. The western older sector of Eburru is covered by upper trachytes which are underlain by lower pantellerite while the caldera on the eastern side is composed of upper pantellerite and upper trachytes. The eastern pantellerites are considered to be the youngest rocks, dating about 400 years (Clarke et al., 1990). The presence of syenite below the entire Kenyan Rift has been suspected, including in Eburru geothermal field; the drilled cores collected from Eburru confirmed a syenitic body at about 2400 m below ground level. The volcanic cones and domes have been referred to as a caldera (Omenda, 1997).

Six wells have been drilled in Eburru (Figure 11). Three out of the six wells discharged and one well, EW-1, is used for production of 2.5 MWe. The fluid chemistry from well EW-1 indicates that Eburru reservoir is non-boiling with a high amount of non-condensable gases and high-salinity brine. Low magnesium and calcium content in the brine reduces the scaling problem in this well with a high chloride level of 956-1976 ppm compared to Olkaria (KPC, 1990).

5.2 The resistivity survey

The geophysical methods applied during the early 1980s included DC soundings (Schlumberger) and gravity leading to the siding of the exploratory wells. In 2006 to 2007, the more advanced geophysical methods, comprising transient electromagnetics (TEM) and magnetotellurics (MT), were applied. A total of 7 TEM and 7 MT soundings were carried out using the Zonge TEM system and MTU-5A Phoenix MT equipment, respectively (Figure 12). The latest survey of April 2013 added 36 MT and 36 TEM soundings using two sets of TerraTEM system and four sets of MTU-5A Phoenix MT equipment.

A total of 43 TEM and 43 MT soundings were analysed to improve the conceptual model of Eburru geothermal field.

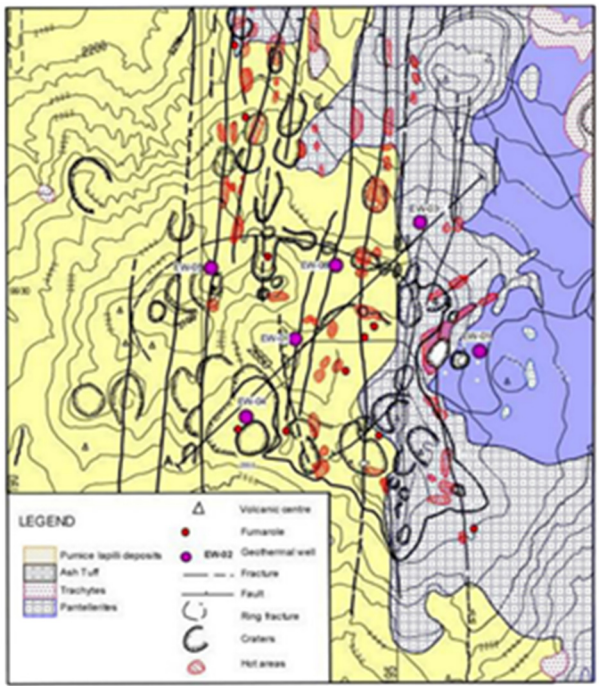

FIGURE 11: Eburru geological map with structures (Omenda and Karingithi, 1993)

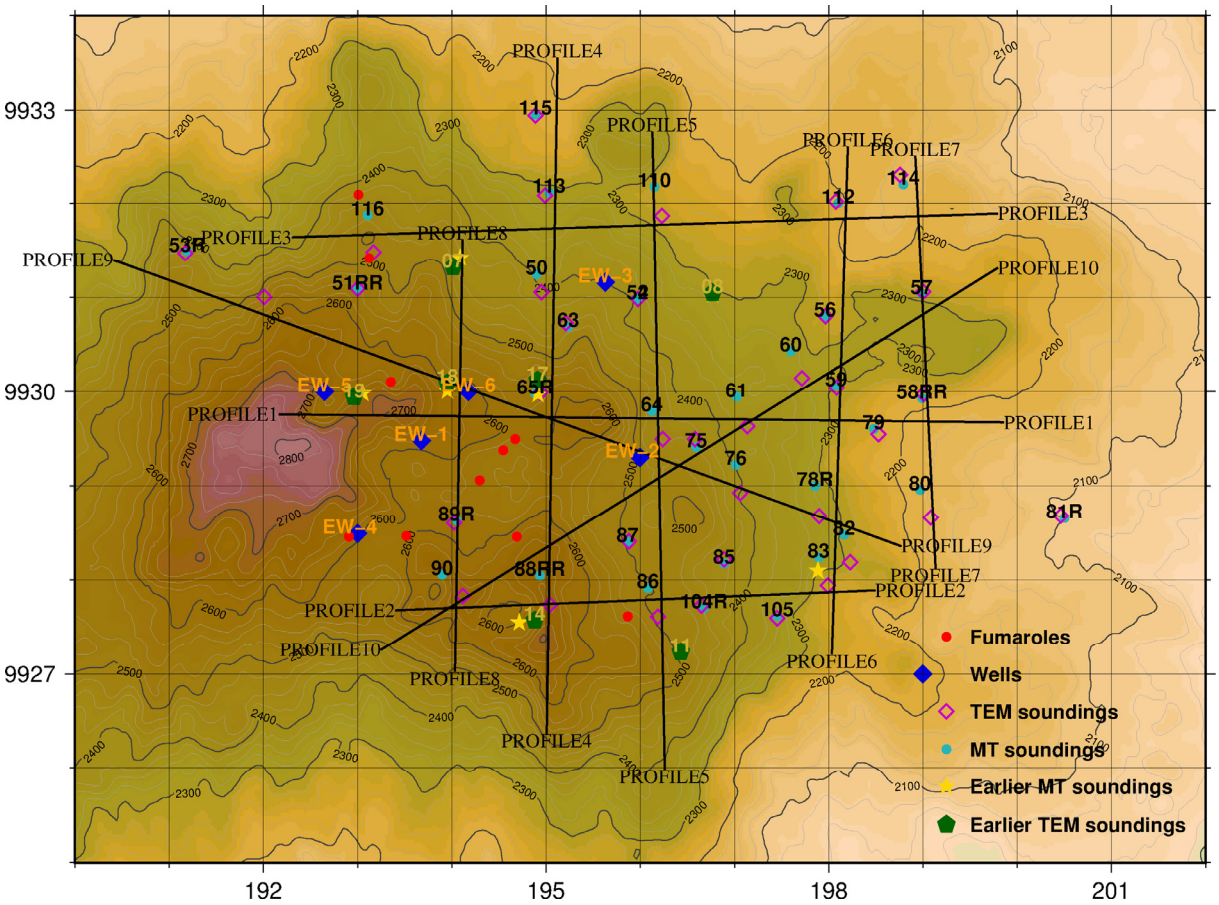

FIGURE 12: Location of MT soundings (black dots) and TEM soundings (inverted triangles); black lines are the cross-sections used in interpreting the resistivity structure of Eburru

6. PROCESSING AND INVERSION OF EBURRU FIELD DATA

MT and TEM data processing is specifically done to suppress various types of noise that affect measurements. It was found that the method used in processing these data could recover response functions from noisy field data. The processed data used in defining the subsurface resistivity structure of the Eburru geothermal field were high-quality data except for a few which were used as bench marks to test the quality of the software in case the field data were noisy.

6.1 Transient electromagnetic data processing

The TerraTEM data collected in Eburru were processed by TemxUSF program, a new version of TEMX for TerraTEM equipment. The program reads the USF file output of TerraTEM and enables a visual editing of data by masking outlier points before the data are used in TEMTD for inversion (Árnason, 2006a).

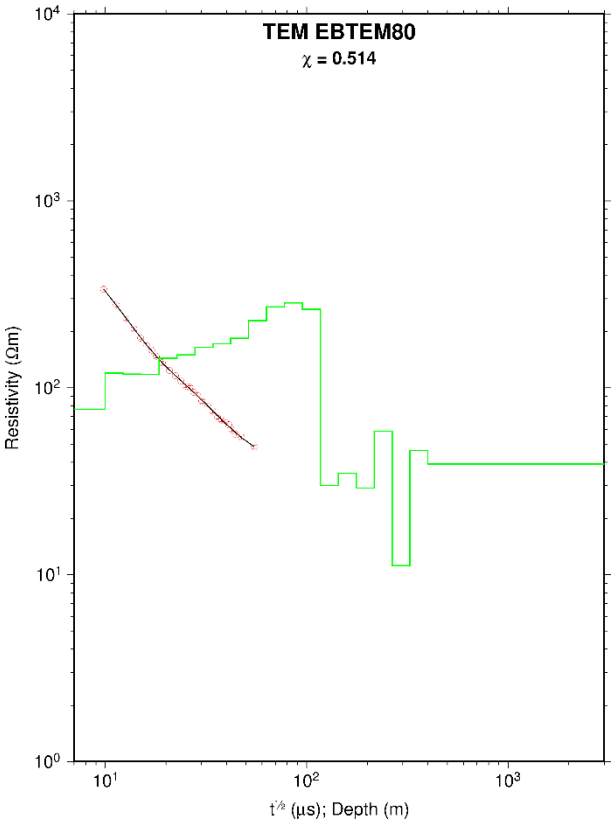

FIGURE 13: 1D inversion of a TEM sounding; χ shows the fit between measured and calculated data

The TEMTD program was used for the Eburru data to perform 1D inversion. In 1D inversion it is assumed that the earth consists of horizontal layers with different resistivity and thicknesses (Figure 13). The program runs on a Linux operational system and can be used for joint inversion of MT and TEM, or inversion of MT or TEM alone. For joint inversion, the program is used to determine the best static shift for MT data and indicate the static shift value, hence solving the shift problem. 1D inversion calculates the layered model and determines how its response best fits the measured data. All the TEM soundings curves and the associated 1D models are given in Appendix I (Omiti, 2013).

6.2 Magnetotelluric data processing

The MT data analysed in this report were acquired using magnetotelluric equipment MTU-5A made by Phoenix Geophysics, Canada. Data were acquired with three different sets of equipment. The initial processing was done by SSMT2000 from Phoenix Geophysics (2005). The software was provided by the equipment manufacturer. This involved editing the parameter file to reflect the setup of the data acquisition and Fourier transforming the resulting time series data to the frequency domain. The MTEditor program was then used to display the phase curves, the apparent resistivity and the auto- and cross powers used to calculate each point of the curve. The program was also used to edit or smooth the data further by removing outliers, considered as noisy data points, on the phase or apparent resistivity curve. The final results from MTEditor were stored in EDI format (Electromagnetic data interchange), ready for inversion in the TEMTD program (Figure 14). Processed data of all the MT soundings are shown in Appendix II (Omiti, 2013).

6.3 Eburru strike analysis

Rose diagrams for the electrical strike, based on the Tipper strike for different period ranges, were analysed for this report. Tipper strikes at shallow depths 0.001-1 s, and greater depths, 1-1000 s, are shown in Figures 15 and 16. The Tipper strike is consistent with the results of 1D joint inversion models with the low resistivity at the centre and the Tipper strike aligned around the low resistivity.

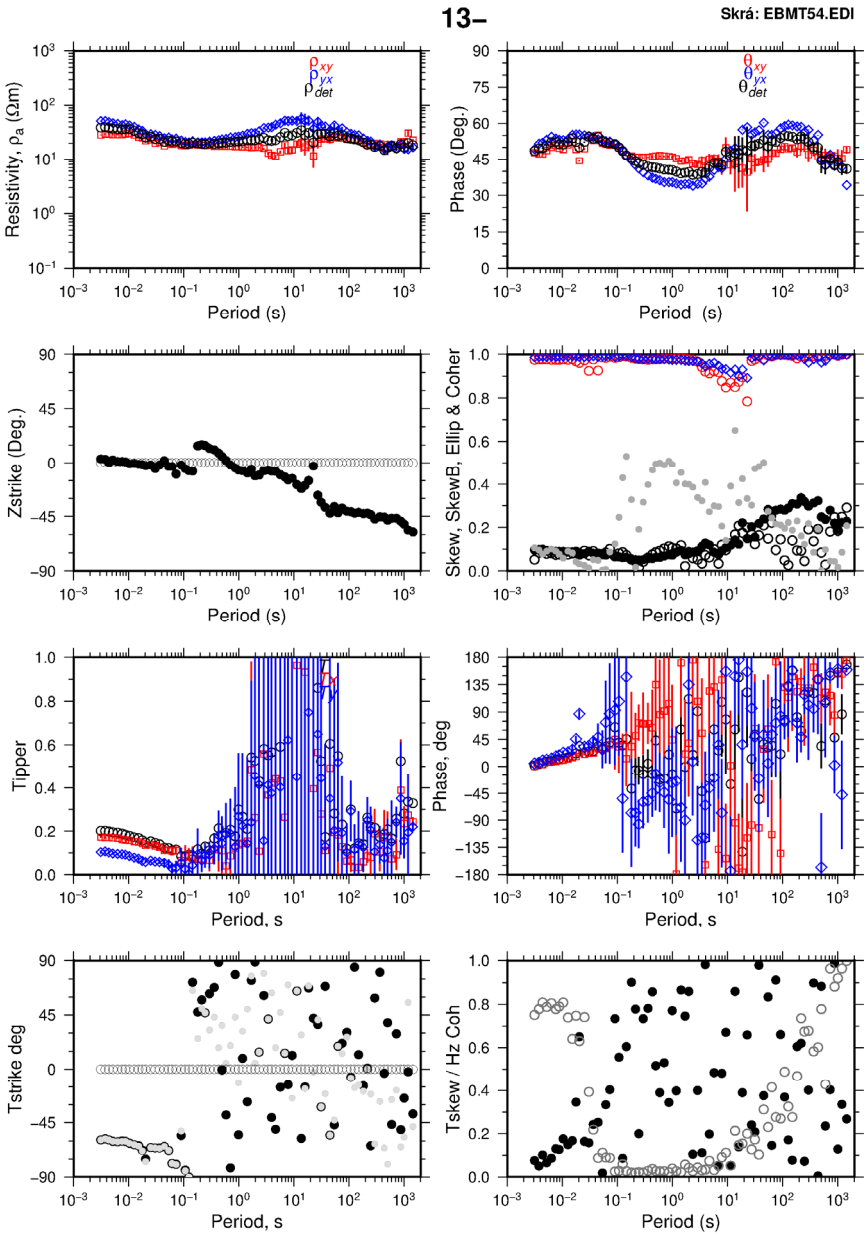

FIGURE 14: MT parameters as extracted from EDI file: apparent resistivity, phase in xy and yx direction and the determinant, electrical strike direction Zstrike, coherence, skew, Tipper, Tipper phase, Tstrike and Tskew

6.4 TEMTD 1D inversion

TEMTD is a program used for 1D inversion of MT data and joint inversion of MT and TEM data. The TEMTD program was written by Knútur Árnason of ISOR (Árnason, 2006b). The program is capable of inverting the apparent phase derived from the MT off-diagonal element tensor (yx and xy modes) and the apparent resistivity (Figure 17). It is also able to calculate the static shift multiplier needed to fit both the TEM and MT data with the same model in joint inversion. It is capable of doing smooth Occam inversion with increasing but fixed layered thicknesses with depth as well as with inverting for resistivity values and thicknesses of layered models. A complete set of all the 1D joint inversion results of each sounding is shown in Appendix III (Omiti, 2013).

6.4.1 Joint Inversion of MT and TEM

As discussed in the next section, MT apparent resistivity is frequently shifted by a multiplicative factor. The shift is constant at all frequencies with no effect on the phase data (Jones, 1988). The amount of static shift depends on the resistivity characteristics beneath the area of study (Berdichevsky and Dmitriev, 1976).

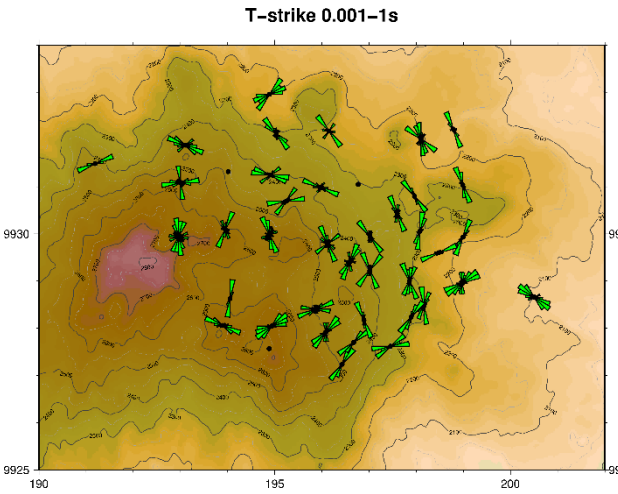

FIGURE 15: Rose diagram for the electrical direction based on the Tipper strike at 0.001-1 s

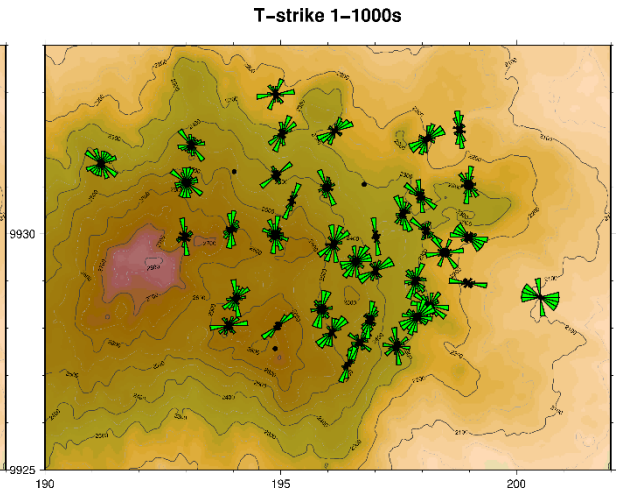

FIGURE 16: Rose diagram for the electrical direction based on the Tipper strike at 1-1000 s

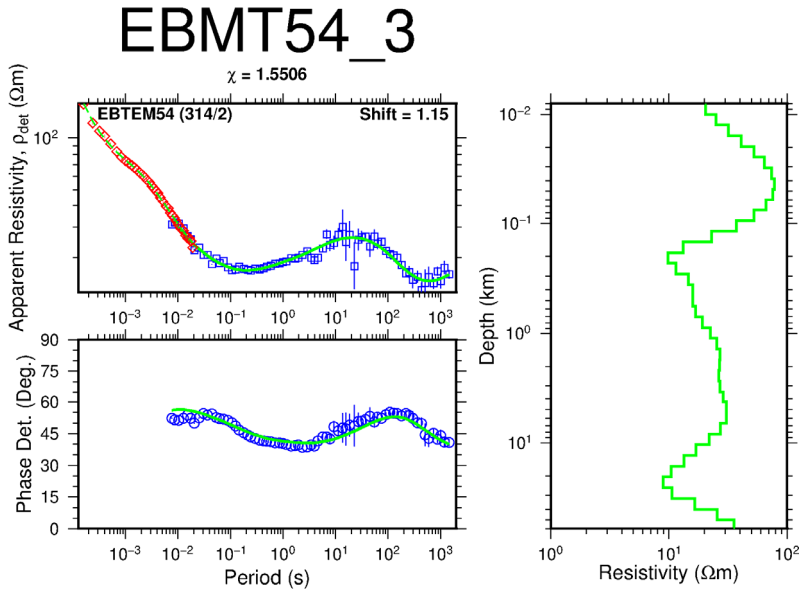

FIGURE 17: 1D Joint inversion of MT and TEM soundings; red and blue symbols on the top left represent the TEM apparent resistivity and the determinant apparent resistivity of the MT soundings, respectively; the bottom panel shows the determinant apparent phase of the MT sounding; the right box shows the results of 1D resistivity inversion model, the green line is the fit of TEM and MT data

TEMTD software was used for jointly inverting MT and TEM data for correction of static shift. Joint 1D Occam inversion of MT and TEM data was performed and the best multiplicative factor or shift parameter of all the MT soundings in Eburru were determined (see Figure 17).

6.5 Static Shift

Near surface inhomogeneities result in the build-up of charges which cause electric field distribution or galvanic distortion to affect the MT data (Chave and Smith, 1994). The distortion manifests itself as a frequency independent and unknown multiplier factor (shift on a log-scale) of the apparent resistivity. The phase, however, is not affected. TEM soundings do not experience the static shift problem; therefore, TEM data are used for static shift correction of MT data collected at the same site. Apparent resistivity processed from MT data can be scaled to fit the TEM curve data or jointly inverted with TEM data.

A total of 43 MT soundings were jointly inverted with TEM data. Figure 18 shows a histogram of shift parameters from the Eburru geothermal field. Most of the MT shifts are less than one, indicating a conductive body underlying the area. All the MT data were shifted, showing the importance of TEM at every MT station. Figure 19 shows a map of the spatial distribution of static shift parameters in Eburru geothermal field, dominated by low shift parameters.

7. RESULTS AND DISCUSSION

Resistivity interpreted from electromagnetic methods or direct current method has been used for geothermal exploration for several years. The correlation between resistivity and drilling results has been done in many drilled geothermal field and shows that the resistivity method can be used to "x-ray" the earth's subsurface (Árnason et al., 2000). The indirect correlation of temperature and resistivity is controlled by the degree of hydrothermal alteration. High-temperature geothermal systems are normally associated with low resistivity resulting from mineral alteration (Árnason et al., 2000). The possibility of using the resistivity method to interpret temperature, permeability and alteration in a geothermal system sometimes resolves the geometry of the geothermal reservoir.

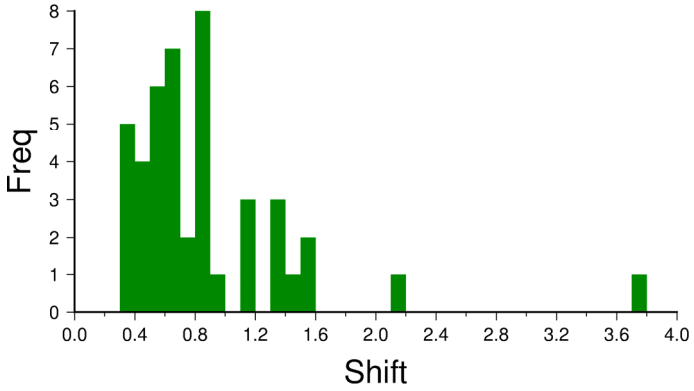

FIGURE 18: A histogram of the static shift parameters for Eburru field

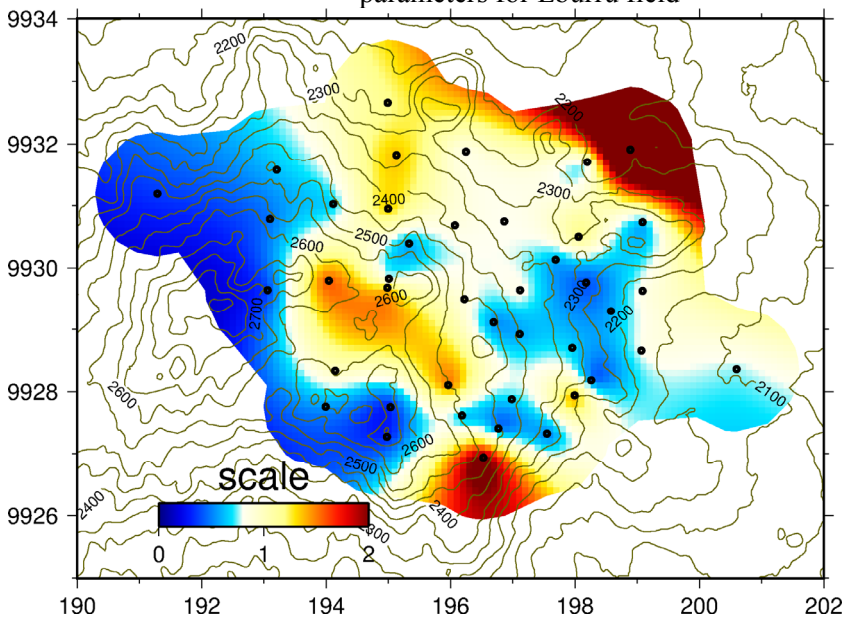

FIGURE 19: Spatial distribution of static shift parameters for determining apparent resistivity in Eburru geothermal field

The study of low-resistivity zones is very essential in the delineation of high-temperature zones targeted for geothermal drilling. The interpretation of Eburru data will take into consideration the structures, the geological setting and the alteration pattern that might influence the area's resistivity distribution. The final models are presented here in two different ways, as iso-resistivity maps for different elevations (depths) and as resistivity cross-sections.

7.1 Cross-sections

Several cross-sections were made in the area, with the locations shown in Figure 12 above. Three cross-sections are in an east-west direction, five in a north-south direction, one in a northeast-southwest direction and the last one in a southeast to northwest direction (Omiti, 2013, Appendix IV). The cross-sections were plotted by the TEMCROSS program (Eysteinsson, 1998) developed at ISOR – Iceland GeoSurvey. The programme plots the resistivity obtained from the 1D inversion.

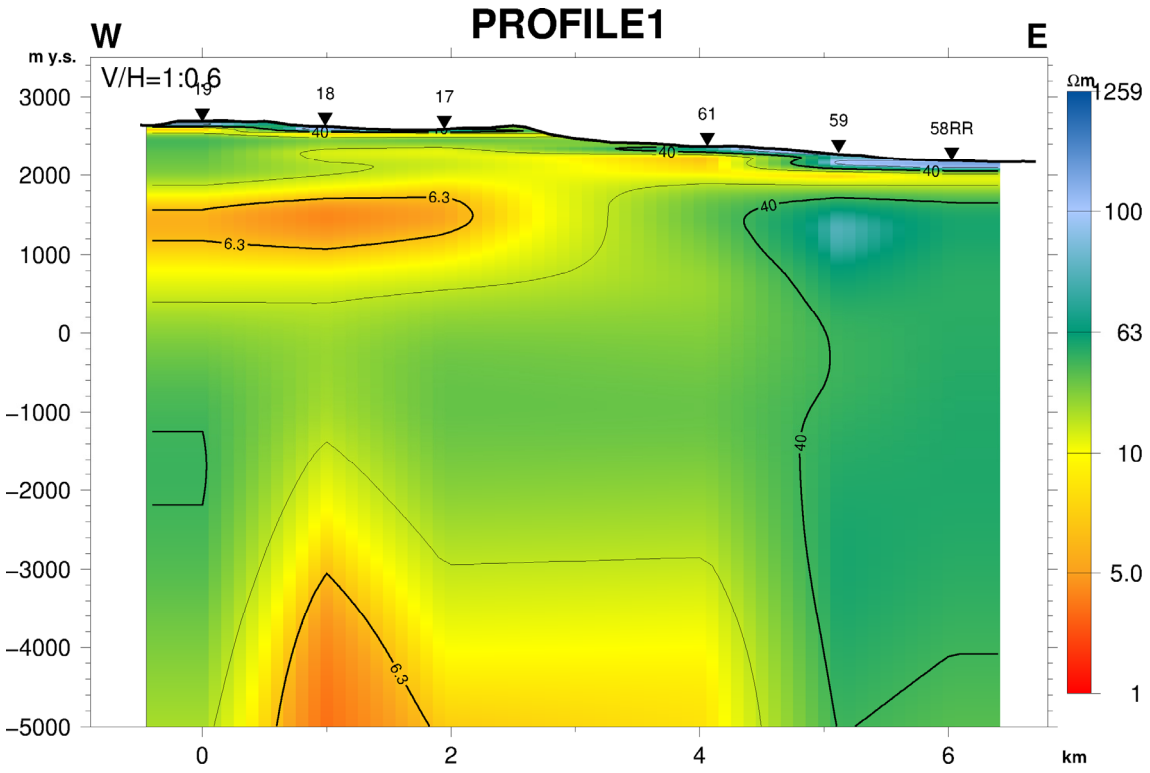

FIGURE 20: Resistivity cross-section in Eburru along profile 1 based on 1D joint inversion of MT and TEM data

Cross-section along profile 1 (Figure 20) has six soundings and is about 7 km long (cuts across well EW-5 and EW-6): It shows a thin resistive layer near the surface along the profile interpreted as unaltered formations underlain by low resistivity less than 10 Ωm, interpreted as due to the effect of geothermal manifestations such as fumaroles. Below this, at 900-1800 m a.s.l., is a conductive cap beneath soundings 19, 18, and 17, of resistivity less that 6 Ωm, interpreted as hydrothermal alteration minerals like zeolites and smectite formed in the temperature range of 100-230°C. It is then underlain by a resistive body, interpreted as high-temperature alteration minerals associated with chlorite and epidote with a formation temperature range between 250 and 300°C. Up-doming low resistivity at 3000 m b.s.l. below soundings 19, 18, and 17 is probably associated with the heat source of Eburru geothermal field. Soundings 59 and 58RR mark the eastern boundary of Eburru geothermal field. A thin conductive layer near the surface is interpreted as the presence of sediments and groundwater and is not associated with geothermal activity. The underlying high resistivity is described as the regsional resistivity outside a geothermal field.

The cross-section along profile 2 (Figure 21) is to the south of well EW-4, 2 km south of profile 1, cuts across five soundings and extends for 5 km. The resistivity distribution of the top layer varies from west to east with a medium resistivity of 10-30 Ωm seen near the surface beneath sounding numbers 90, 88R and 86, interpreted as near surface alteration, and a resistive layer of 100 Ωm beneath soundings 85 and 83, interpreted as unaltered formation near the surface. The low resistivity to the west continues downwards and is underlain by a resistive body of about 50 Ωm at 900 m a.s.l. down to 2100 m b.s.l., interpreted as a chlorite-epidote zone due to high-temperature geothermal alteration. The eastern part below soundings 85 and 83 shows a very thin layer of low resistivity at about 2200 m a.s.l., interpreted as being due to sedimentary deposits and groundwater effect. It is then underlain by high resistivity down to a depth beyond 10,000 m b.s.l., interpreted as normal resistivity outside the geothermal field and, hence, outside the boundary of the resource area to the east.

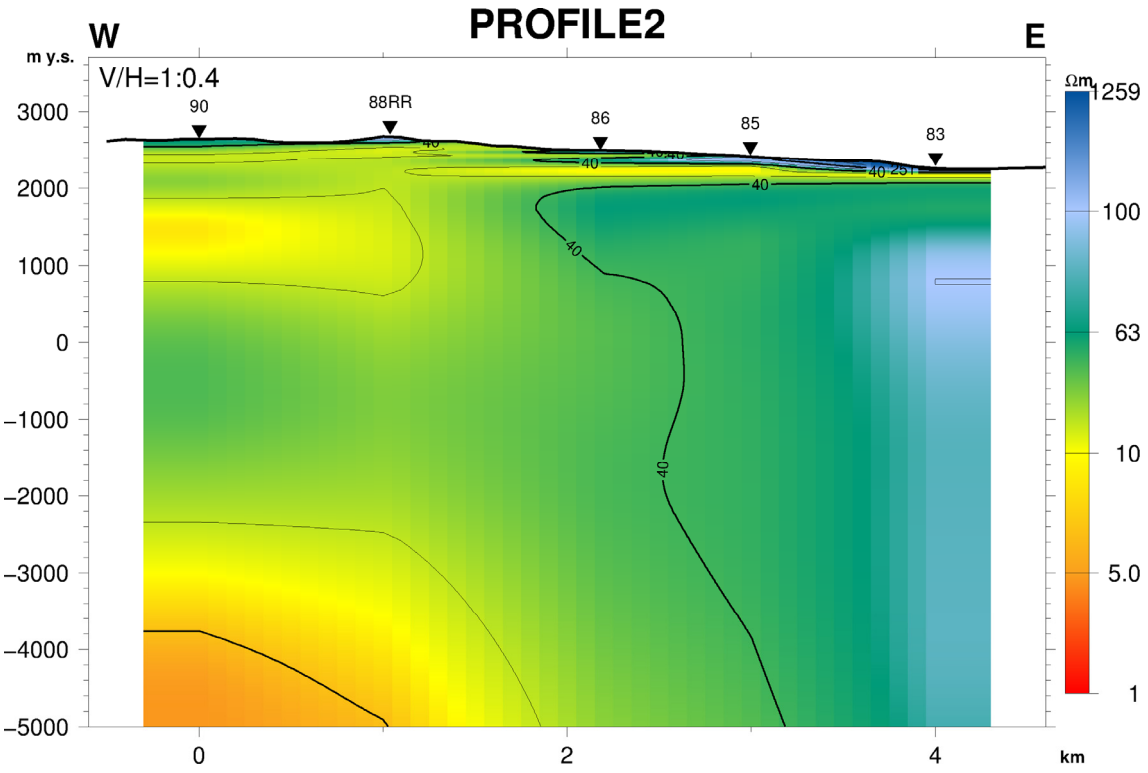

FIGURE 21: Resistivity cross-section in Eburru along profile 2 based on 1D joint inversion of MT and TEM data

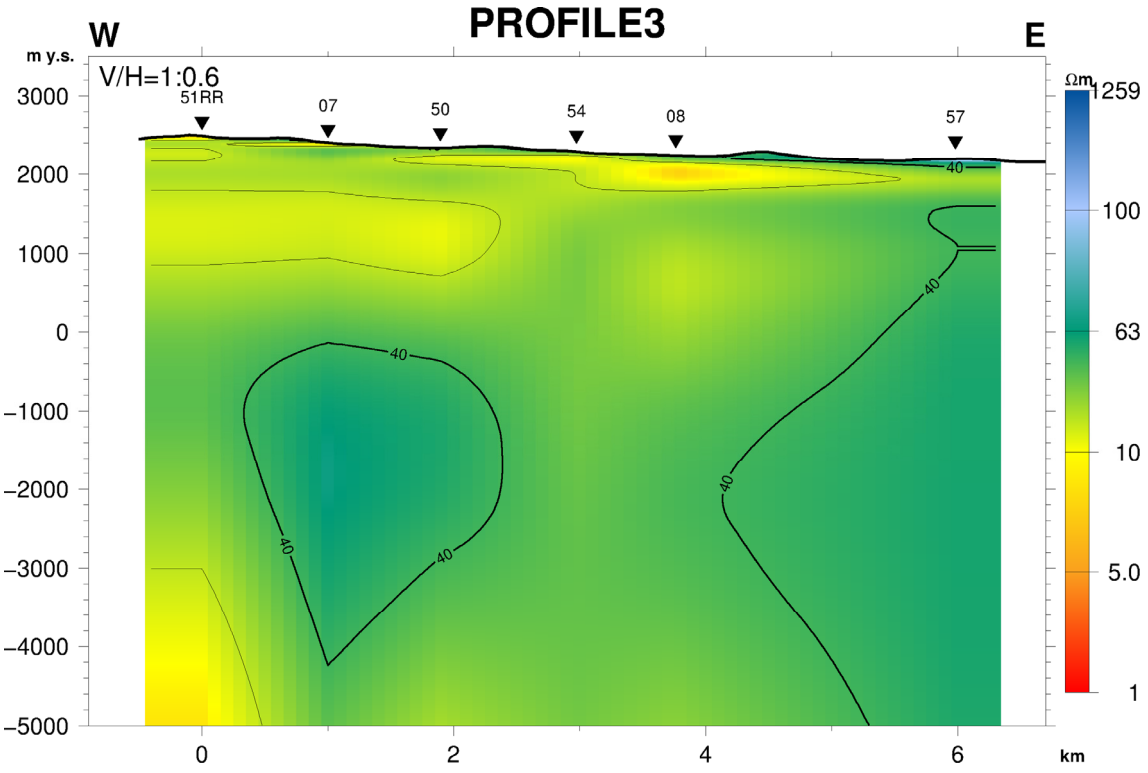

FIGURE 22: Resistivity cross-section in Eburru along profile 3 based on 1D joint inversion of MT and TEM data

The cross-section along profile 3 (Figure 22) dissects the area in a west-east direction, cutting across six soundings in the northern part of the study area, close to well EW-3. The resistivity pattern of the area

indicates a close proximity to the northern boundary of the geothermal field. Resistivity pattern related to low- and high-temperature alteration minerals is not as well evident in the western side of the cross-section as in profile 1. The eastern side shows the regional resistivity outside the geothermal field, indicating the boundary.

Profile 4 cross-section (Figure 23) cuts the area in a north-south direction. It is about 6 km long and includes seven soundings. The resistivity pattern shows the northern boundary below soundings 115 and 113. The southern part has a thin layer of high resistivity near the surface, indicative of unaltered minerals, overlying a uniform fairly low resistivity of about 10 Ωm, indicative of altered minerals due to steam condensate from a hot upflow from the underlying resistive layer, interpreted as high-temperature altered rock.

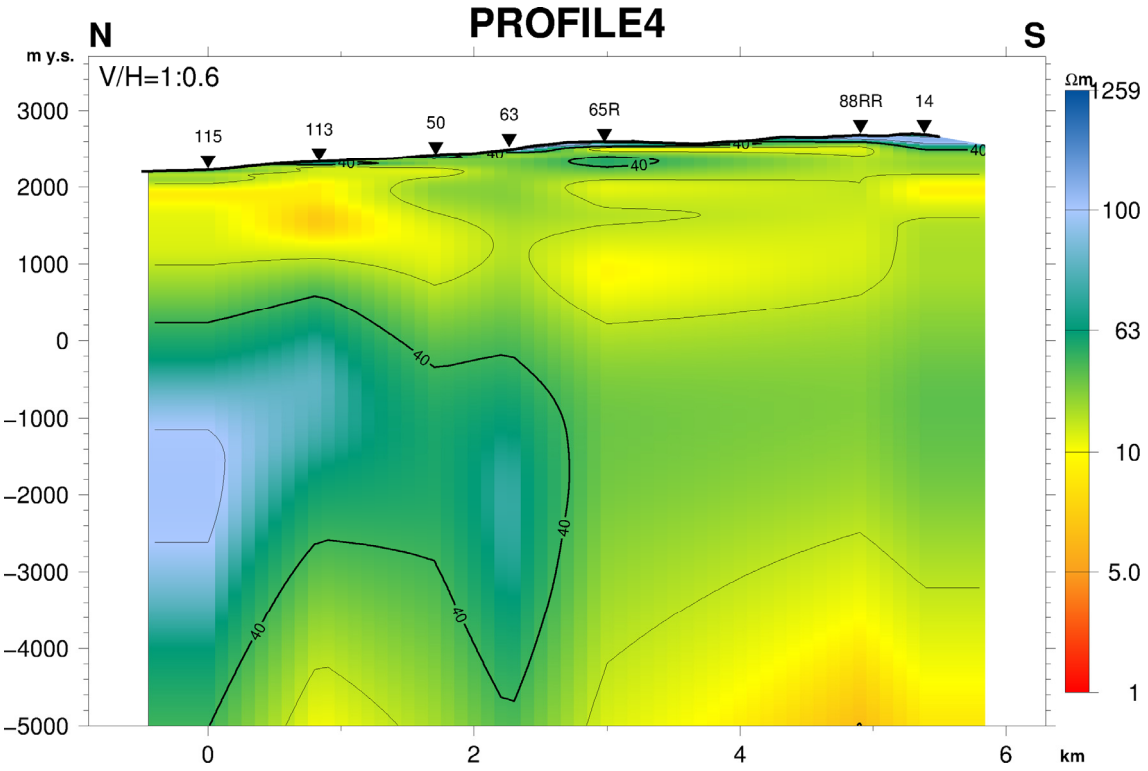

FIGURE 23: Resistivity cross-section in Eburru along profile 4 based on 1D joint inversion of MT and TEM data

The cross-section along profile 8 (Figure 24) is about 4.5 km long. It includes four soundings in a north-south direction and passes close to well EW-1 and EW-6. The distribution of the resistivity in this cross-section clearly depicts resistivity of a high-temperature field. At the top is a thin layer of high resistivity near the surface, signifying unaltered rocks overlying the low resistivity of about 10 Ωm, interpreted as resulting from geothermal activity. A pocket of low resistivity (< 5 Ωm) below soundings 18 and 89R, interpreted as a smectite-zeolite zone, could indicate low-temperature alteration from a hot upflow condensate from an underlying resistive layer, interpreted as a chlorite-epidote zone associated with high-temperature alteration minerals, is in agreement with the temperature log in well EW-1. The temperature in well EW-4 is in disagreement with the subsurface resistivity presumably due to the fossil effect in the reservoir towards the southern boundary, indicating cooling of the reservoir. All the cross-sections are shown in Appendix IV (Omiti, 2013).

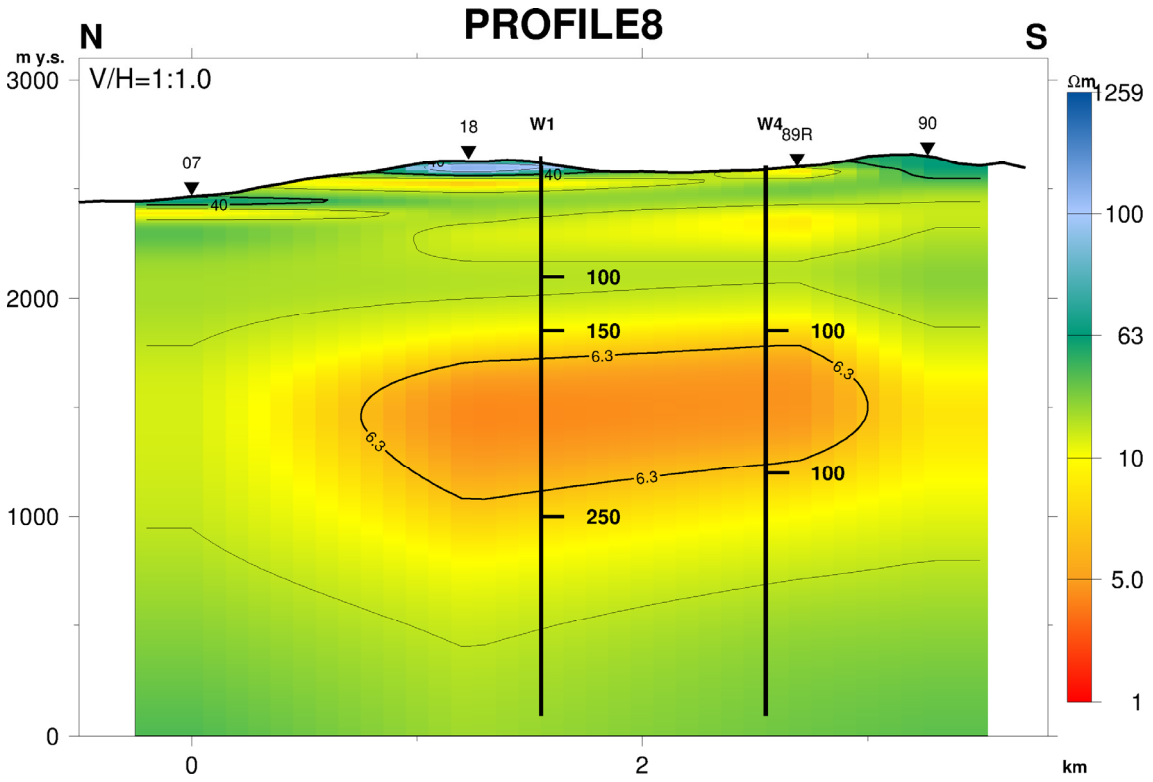

FIGURE 24: Resistivity cross-section in Eburru along profile 8 based on 1D joint inversion of MT and TEM data

7.2 Iso-resistivity maps

Iso-resistivity maps were constructed from TEMMAP program (Eysteinsson, 1998) to display the resistivity at different depths in Eburru. Analysis of the conductance, which is a product of the resistivity and thickness, was also done.

Resistivity map at 2000 m a.s.l. (Figure 25): At about 500 m below the ground level, the map shows a fairly uniform resistivity of about 10 Ωm. The fairly low resistivity can be interpreted as due to hydrothermal alterations lining fractures in rocks. Low resistivity on the eastern, northern and northwest boundaries is due to sediments and groundwater effect.

Resistivity map at 1500 m a.s.l. (Figure 26): At about 1500 m below the ground level, this map shows a fairly low resistivity (< 10 Ωm) except for the eastern boundary. The fairly low resistivity is interpreted as low-temperature alteration minerals like smectite or zeolites and also confirms the presence of geothermal fluid.

Resistivity map at 500 m a.s.l. (Figure 27): At about 2500 m below the ground level, this map shows high resistivity defining the reservoir of Eburru. The high resistivity of > 40 Ωm in the central part is interpreted as due to the high-temperature alteration minerals, chlorite and epidote. The southeast, northeast and northwest parts show very high resistivity, of >100 Ωm, defining areas outside the geothermal system.

Resistivity map at 1500 m b.s.l. (Figure 28): At about 4000 m below the ground level, low resistivity spreads from the southwest, interpreted to be connected to the heat source of Eburru geothermal field. The high resistivity of the outer layer persists downward, an indication of the boundary and areas outside the geothermal system.

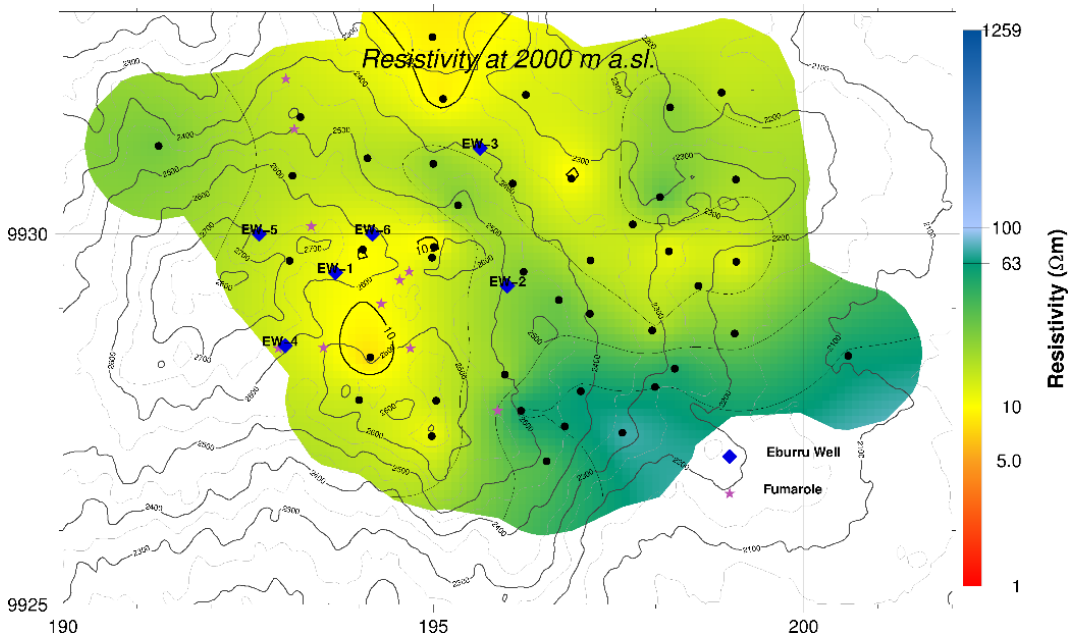

FIGURE 25: Resistivity iso-map at 2000 m a.s.l. of Eburru geothermal field, black dots denote MT soundings

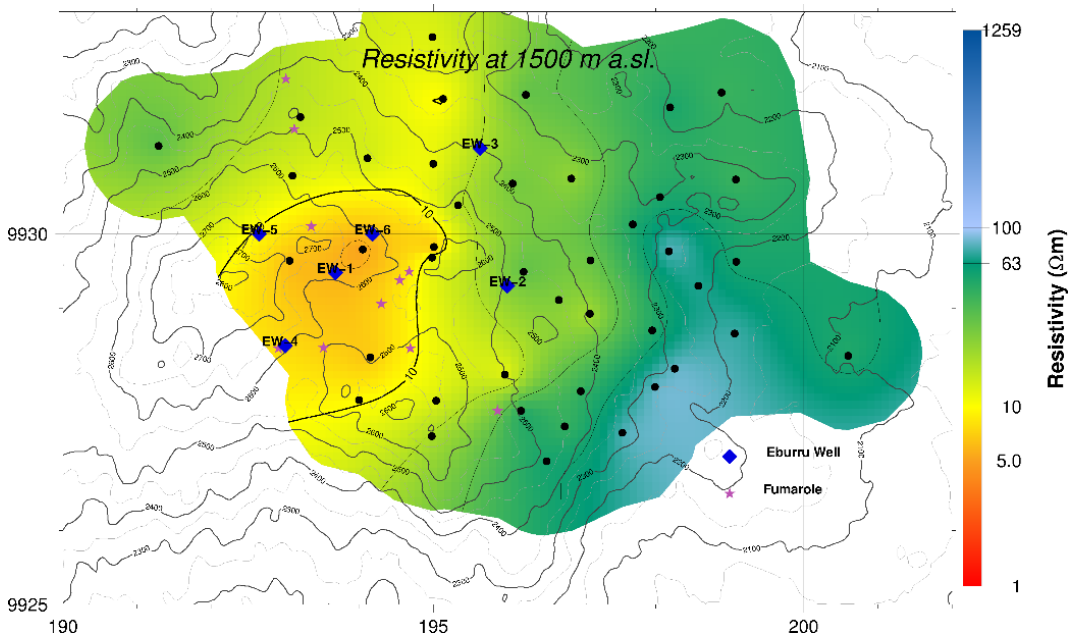

FIGURE 26: Resistivity iso-map at 1500 m a.s.l. of Eburru geothermal field

Resistivity map at 2500 m b.s.l. (Figure 29): At about 5000 m below the ground level, the central delineated low resistivity is associated with the heat source of Eburru geothermal field. The boundary of the resource is evident in the boundary between the low resistivity and high resistivity, with the very high resistivity defining areas outside the geothermal system.

Resistivity map at 10,000 m b.s.l. (Figure 30): At about 12,500 m below the ground level, there is not as much change as in Figure 29 except for the persistent decrease of resistivity in the southwest side of the centre, an indication of an increase in the conductor downwards towards the suspected deep seated heat source (magma chamber) within the volcano. Three wells drilled above the heat source discharged (EW-

1, EW-6 and EW-4) and the remaining three wells drilled outside the heat source did not discharge, indicating the importance of a geophysical survey before exploration drilling.

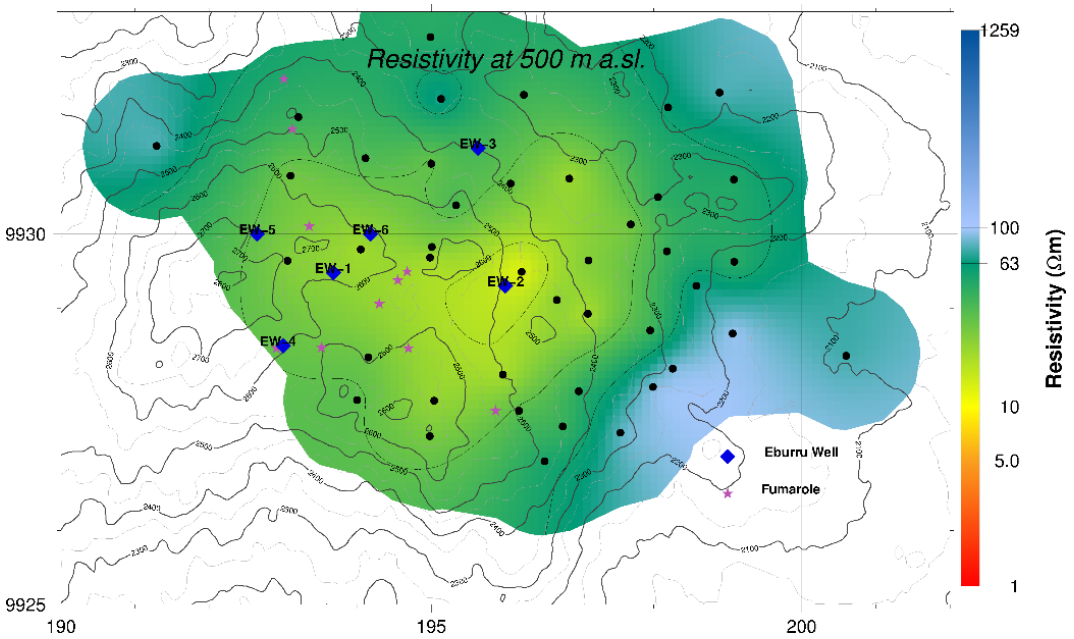

FIGURE 27: Resistivity iso-map at 500 m a.s.l. of Eburru geothermal field

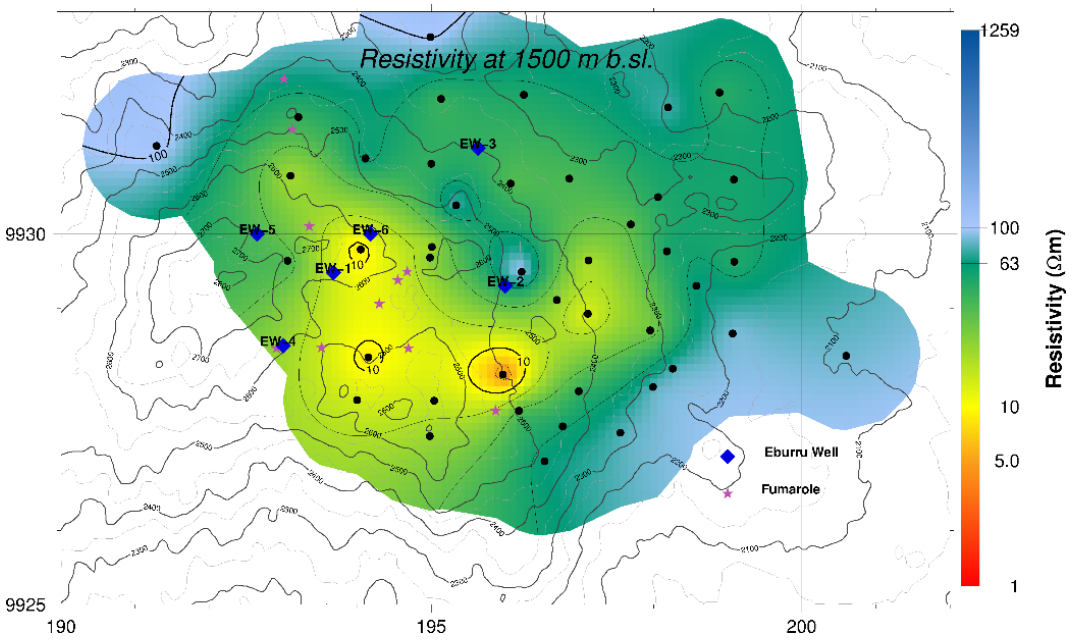

FIGURE 28: Resistivity iso-map at 1500 m b.s.l. of Eburru geothermal field

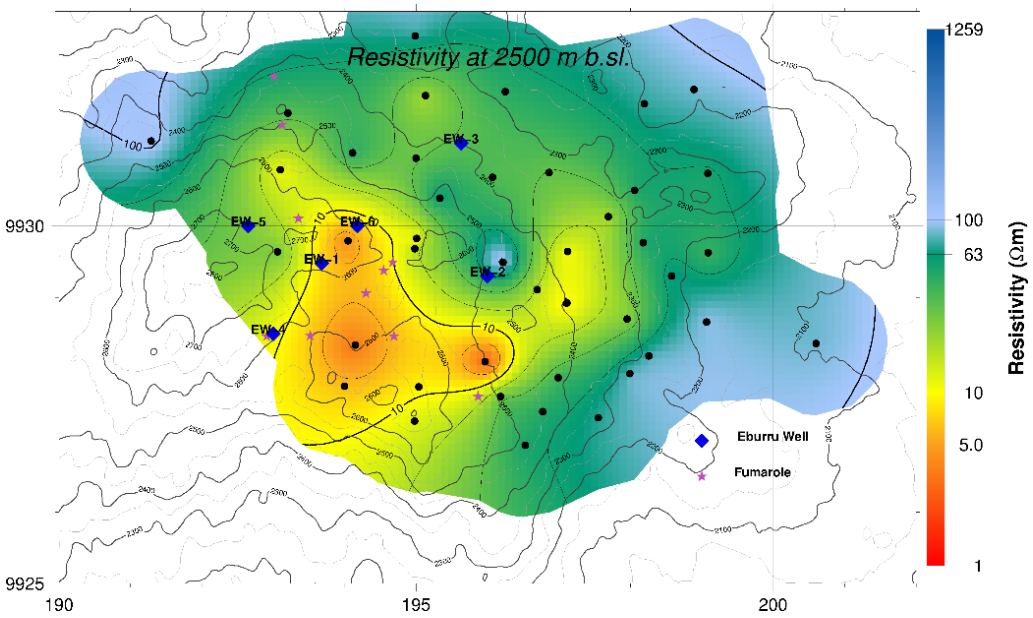

FIGURE 29: Resistivity iso-map at 2500 m b.s.l. of Eburru geothermal field

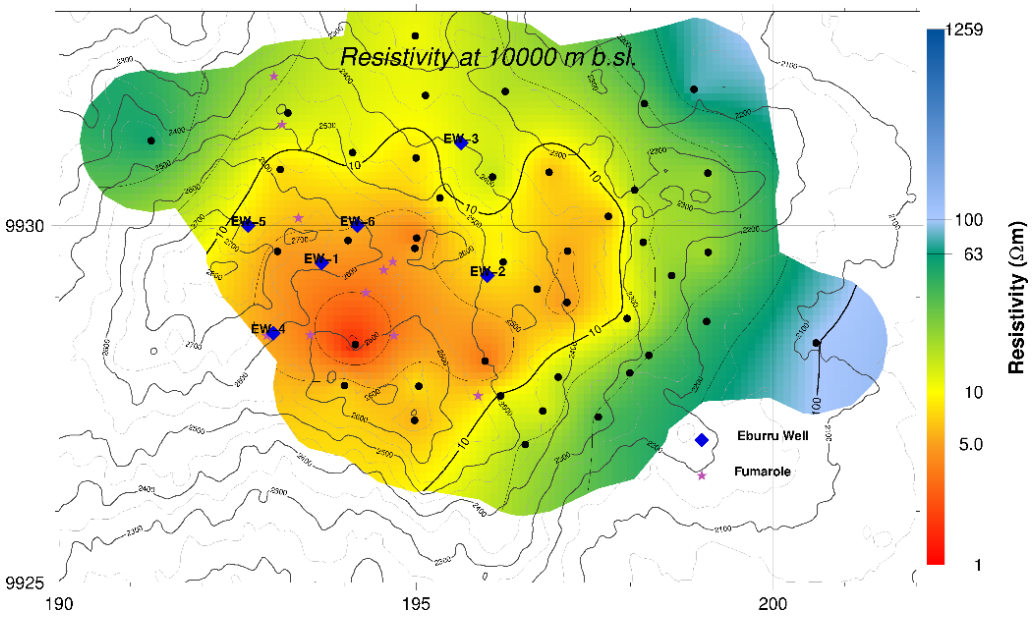

FIGURE 30: Resistivity iso-map at 10,000 m b.s.l. of Eburru geothermal field

8. CONCLUSIONS AND RECOMMENDATIONS

From the Eburru integrated data interpretation of 1D joint inversion of MT and TEM data, the following resistivity layers were observed in cross-sections and iso-maps:

- A very thin layer of high near-surface resistivity (> 60 Ωm) covering almost the entire area, interpreted as unaltered formations and superficial deposits;
- It is followed by a uniform near-surface low-resistivity layer (< 10 Ωm) resulting from geothermal acivity, such as fumaroles;
- A second layer of low resistivity (< 6 Ωm) is evident in the central and southwest parts, associated with smectite and zeolite alteration which formed as a result of hydrothermal alteration;

- It is followed by a resistive layer (> 30 Ωm) at about 2500 m b.g.l., associated with resistive high-temperature alteration minerals like epidote and chlorite which define the geothermal system of Eburru;
- A good deep conductor (< 10 Ωm), indicating the probable heat source of Eburru geothermal field, is well evident in the southwest towards the centre.

The interpreted data clearly delineates the Eburru geothermal resource boundary except to the southwest where the resource seems to be close to the surface. It is, therefore, recommended that more MT and TEM data be collected in the western and southwest parts of the study area in order to delineate the exact boundaries of the resource field.

ACKNOWLEDGEMENTS

I owe my sincere appreciation to outgoing Director, Dr. Ingvar Birgir Fridleifsson, and the new Director, Mr. Lúdvík S. Georgsson, for awarding me this scholarship. I would also like to thank Ms. Málfrídur Ómarsdóttir, Mr. Ingimar G. Haraldsson, Mr. Markús A.G. Wilde, Ms. Thórhildur Ísberg and all of the ISOR staff for helping and guiding me during the training period. Special thanks go to my supervisors, Mr. Gylfi Páll Hersir and Mr. Knútur Árnason, for always being there for me and working with me full time during this research work. I would also like to express my gratitude to my classmates - we had fruitful discussions. To my family, thanks for your prayers and love throughout my entire training in Iceland. Lastly and the greatest of all, thanks go to God, for care and sustenance throughout my work.

REFERENCES

Archie, G.E., 1942: The electrical resistivity log as an aid in determining some reservoir characteristics. *Tran. AIME, 146,* 54-67.

Árnason, K., 1989: *Central loop transient electromagnetic sounding over a horizontally layered earth*. Orkustofnun, Reykjavík, report OS-89032/JHD-06, 129 pp.

Árnason, K., 2006a: *TemX short manual.* ÍSOR – Iceland GeoSurvey, Reykjavík, internal report, 17 pp.

Árnason, K., 2006b: *TEMTD, a programme for 1D inversion of central-loop TEM and MT data*. Short manual. ÍSOR – Iceland GeoSurvey, Reykjavík, internal report, 17 pp.

Árnason, K., Karlsdóttir, R., Eysteinsson, H., Flóvenz, Ó.G., and Gudlaugsson, S.Th., 2000: The resistivity structure of high-temperature geothermal systems in Iceland. *Proceedings of the World Geothermal Congress 2000*, *Kyushu-Tohoku, Japan,* 923-928.

Berdichevsky, M.N., and Dmitriev, V.I., 1976: Distortion of magnetic and electric fields by near-surface lateral inhomogeneities. *Acta Geodaet. Geophys. et Montanist. Acad. Sci. Hung*., *11,* 447-483.

Cagniard, L., 1953: Basic theory of the magneto-telluric method of geophysical prospecting. *Geophysics, 18,* 605-635.

Chave, A.D., and Smith, J.T., 1994: On electric and magnetic galvanic distortion tensor decomposition. *J. Geophys. Res.*, 99-B3, 4669-4682.

Clarke, M.C.G., Woodhall, D.G., Allen, D., and Darling G., 1990: *Geological, volcanological and hydrogeological controls on the occurrence of geothermal activity in the area surrounding Lake Naivasha, Kenya, with coloured 1:100 000 geological maps.* Ministry of Energy, Nairobi, 138 pp.

Dakhnov, V.N., 1962: Geophysical well logging. *Q. Colorado Sch. Mines, 57-2*, 445 pp.

Encyclopaedia Britannica, 2010: Solar wind. Encyclopaedia Britannica Online, webpage: *www.britannica.com/EBchecked/topic/1589681/Solar-Dynamics-Observatory*.

Everett, J.E., and Hyndman, R.D., 1967: Geomagnetic variations and electrical conductivity structure in southwestern Australia. *Phys. Earth Planet. Inter., 1,* 24-34.

Eysteinsson, H., 1998: *TEMRESD, TEMMAP and TEMCROSS plotting programs.* ÍSOR - Iceland GeoSurvey, unpublished programs and manual.

Flóvenz, Ó.G., Hersir, G.P., Saemundsson, K., Ármannsson, H., and Fridriksson Th., 2012: Geothermal energy exploration techniques. In: Sayigh, A., (ed.), *Comprehensive renewable energy, vol. 7.* Elsevier, Oxford, 51-95.

Flóvenz, Ó.G., Spangerberg, E., Kulenkampff, J., Árnason, K., Karlsdóttir, R., Huenges, E., 2005: The role of electrical interface conduction in geothermal exploration. *Proceedings of the World Geothermal Congress 2005, Antalya, Turkey,* 9 pp.

Henley, R.W., and Ellis, A.J., 1983: Geothermal systems ancient and modern - a geochemical review. *Earth-Science Reviews, 19-1,* 1-50.

Hersir, G.P., and Björnsson, A., 1991*: Geophysical exploration for geothermal resources. Principles and applications.* UNU-GTP, Iceland, report 15, 94 pp.

Jones, A.G., 1988: Static shift of magnetotelluric data and its removal in a sedimentary basin environment. *Geophysics, 53-7*, 967-978.

Kaufman, A.A., and Keller, G.V., 1981: *The magnetotelluric sounding method.* Elsevier Scientific Publishing Co., Amsterdam, 595 pp.

Kaufman A.A., and Keller, G.V., 1983: *Frequency and transient sounding. Methods in Geochemistry and Geophysics, 16.* Elsevier Scientific Publishing Co., Amsterdam, 685 pp.

KPC, 1990: *Olkaria West field information report.* STRM, Kenya Power Company, Ltd., internal report, 240 pp.

Mehegan, J.M., Robinson, P.T., and Delaney, J.R., 1982: Secondary mineralization and hydrothermal alteration in the Reydarfjördur drill core, eastern Iceland. *J. Geophysical Research, 87-Nb8*, 6511-6524.

Omenda, P.A., 1997: *The geochemical evolution of Quaternary volcanism in south-central portion of the Kenya Rift.*University of Texas, El Paso, PhD thesis, 218 pp.

Omenda, P.A., and Karingithi, C.W., 1993: Hydrothermal model of Eburru geothermal field, Kenya. *Geoth. Res. Council, Trans., 17*, 155-160.

Omiti, A.O., 2013: *Appendices to the report: "Resistivity structure of the Eburru geothermal field, Kenya, described through 1D joint inversion of MT and TEM data".* UNU-GTP, Iceland, report 26 appendices, 104 pp.

Phoenix Geophysics, 2005*: Data processing user guide*. Phoenix Ltd., users guide.

Quist, A.S., and Marshall, W.L., 1968: Electrical conductances of aqueous sodium chloride solutions from 0 to 800°C and at pressures to 4000 bars. *J. Phys. Chem., 72,* 684-703.

Velador, J.M., Omenda, P.A., and Anthony, E.Y., 2002: Geology and the origin of trachytes and pantellerites from the Eburru volcanic field, Kenya Rift. *Paper presented at the AGU Fall Meeting 2002.*

Vozoff, K., 1991: The magnetotelluric method. In: Nabighian, M.N (ed.), *Electromagnetic methods. Applied Geophysics, 2,* 641-711.

Zhdanov, M.S., and Keller, G.V., 1994: *The geoelectrical methods in geophysical exploration.* Elsevier Scietific Publishing Co., Amsterdam, 873 pp.